A Methodology for Initializing Soil Moisture in a Global Climate Model: Assimilation of Near-Surface Soil Moisture Observations

[1,2]Jeffrey P. Walker and [1]Paul R. Houser

[1]*Hydrological Sciences Branch, Laboratory for Hydrospheric Processes, NASA's Goddard Space Flight Center, Greenbelt, MD, USA.*

[2]*Goddard Earth Sciences and Technology Center*

Submitted to:

Journal of Geophysical Research - Atmospheres

28 August 2000

Revised:

15 February 2001

Corresponding Author:

Jeffrey P. Walker

Abstract

Due to its long-term persistence, accurate initialization of land surface soil moisture in fully-coupled global climate models has the potential to greatly increase the accuracy of climatological and hydrological prediction. To improve the initialization of soil moisture in the NASA Seasonal-to-Interannual Prediction Project (NSIPP), a one-dimensional Kalman filter has been developed to assimilate near-surface soil moisture observations into the catchment-based land surface model used by NSIPP. A set of numerical experiments was performed using an uncoupled version of the NSIPP land surface model to evaluate the assimilation procedure. In this study, "true" land surface data were generated by spinning-up the land surface model for 1987 using the International Satellite Land Surface Climatology Project (ISLSCP) forcing data sets. A degraded simulation was made for 1987 by setting the initial soil moisture prognostic variables to arbitrarily wet values uniformly throughout North America. The final simulation run assimilated the synthetically generated near-surface soil moisture "observations" from the true simulation into the degraded simulation once every 3 days. This study has illustrated that by assimilating near-surface soil moisture observations, as would be available from a remote sensing satellite, errors in forecast soil moisture profiles as a result of poor initialization may be removed, and the resulting predictions of runoff and evapotranspiration improved. After only 1 month of assimilation the root mean square error in the profile storage of soil moisture was reduced to 3%v/v, while after 12 months of assimilation the root mean square error in the profile storage was as low as 1%v/v.

1 INTRODUCTION

Due to the long-term persistence of moisture content in the land surface, its accurate initialization in fully-coupled global climate models has the potential for significant improvement in climatological and hydrological prediction. Knowledge of soil moisture content in the top few meters has been shown to influence the prediction of precipitation [*Koster and Suarez*, 1995] and atmospheric circulations [*Fast and McCorcle*, 1991], through its control on partitioning of the available energy into latent and sensible heat exchange [*Delworth and Manabe*, 1989; *Shukla and Mintz*, 1982]. Furthermore, the effects of evaporative dependence on soil moisture content have been observed up to 1km above the earth's surface [*Fast and McCorcle*, 1991]. The presence of horizontal gradients in soil moisture content have been found by *Fast and McCorcle* [1991] to induce circulations similar to sea breezes in the absence of synoptic forcing, which feedback to modify both the spatial distribution and intensity of precipitation. Moreover, *Koster and Suarez* [1995] have found that sea surface temperatures have a much smaller effect on precipitation prediction over land than the land surface soil moisture content, particularly in the tropics and mid-latitudes. The effect of land surface soil moisture content on variation in annual precipitation over continents has been found to be particularly strong during summer when moist convection dominates. In addition, *Delworth and Manabe* [1989] have found that spring-time soil moisture content can have a substantial influence on the summer climate at mid-latitudes.

The current soil moisture content and its distribution influence not only the current climatic conditions, but also future climate through its long-term persistence or memory effect [*Beljaars et al.*, 1996]. Because anomalies of soil moisture content are persistent on seasonal-to-interannual time scales, they create persistent anomalous fluxes of latent and sensible heat,

thereby increasing the persistence of near-surface atmospheric relative humidity and temperature [*Delworth and Manabe*, 1989]. Such persistence has been observed by *Koster and Suarez* [1995] in areas of high soil moisture content with high evaporation rates. In these areas, high soil moisture content instigates increased precipitation and thereby amplifies precipitation anomalies. *Delworth and Manabe* [1988, 1989] have found that smaller values of potential evaporation (which typically decreases poleward) are correlated with more slowly changing anomalies of soil moisture content (with longer time scales). In the tropics and during the summer season, however, larger values of potential evaporation allow fluctuations of soil moisture content to have a substantial effect on the variability of the lower atmosphere [*Delworth and Manabe*, 1989].

Soil moisture content and its spatial distribution clearly influences land surface processes with the potential to severely impact atmospheric variability, which can have a major influence on climate forecasts. Thus, there is a demonstrated need for routine observations of soil moisture content and its distribution, particularly for initialization of climate predictions with a global climate model. The collection of routine soil moisture observations has been curtailed primarily by the extreme heterogeneity of soil properties, topography, land cover, evaporation and precipitation, causing soil moisture content to be highly variable both spatially and temporally. Consequently, the value of operational monitoring of soil moisture content by in-situ methods is rather limited for global scale problems. Currently, remote sensing methods provide the most feasible capability for providing the necessary soil moisture measurements for initialization of the soil moisture states in global climate models, as they average out small-scale variability to better sample the climate-relevant soil moisture patterns.

Global measurements of soil moisture content have been made with the C-band radiometer on the Scanning Multifrequency Microwave Radiometer (SMMR) instrument [M. Owe, personal comunication, 2001] that flew during 1978 to 1987. Current passive microwave satellite instruments, Special Sensor Microwave Imager (SSM/I) and Tropical Rainfall Measuring Mission (TRMM), have only higher frequency radiometers, making soil moisture measurement problematic. However, the Advanced Microwave Scanning Radiometer for the Earth observing system (AMSR-E) instruments due for launch in the near future on the EOS Aqua and ADEOS-II satellites will have C-band radiometers, once again making global measurement of soil moisture possible. An L-band radiometer, the optimal wavelength for soil moisture measurement, is not likely to be in space before 2005. Whilst passive microwave instruments currently have a large footprint, 150 km for SMMR and 60 km for AMSR-E, global measurement of soil moisture content from these instruments is less problematic than for the active microwave instruments with footprints on the order of 10's m. Furthermore, due to over-sampling, the passive microwave measurements may generally be interpolated to a finer resolution (50km for SMMR and 25km for AMSR-E). Moreover, the land surface component of current-day global climate models are typically run with a spatial resolution on the order of 50 to 100 km, which is compatible with the scale of passive microwave measurements.

Soil moisture remote sensing, however, is limited to measurement of soil moisture content in the near-surface layer of soil, consisting of the top few centimeters at most. These upper few centimeters in the soil are the most exposed to the atmosphere, and vary rapidly in soil moisture content, on the order of hours [*Raju et al.*, 1995; *Capehart and Carlson*, 1997] in response to rainfall and evaporation. In fact, the soil surface may change from wet to dry within a period of 1 or 2 days [*Jackson et al.,* 1976], with deeper soil moisture content changing more

slowly. Thus to be useful for climatic and meteorological studies, remote sensing information must be related to the complete soil moisture profile in the unsaturated zone, as any individual observation will largely reflect the climatic effects of the last few hours, rather than the average for the inter-observation period. Therefore, for remote sensing observations to be valuable in applications, methods must be developed to estimate the *soil moisture profile (top few meters of soil)* using the *near-surface (top few centimeters)* measurements of soil moisture content that these sensors provide.

Only a small number of studies have used remotely sensed near-surface soil moisture measurements as either input to a land surface model [*Jackson et al.*, 1981; *Prevot et al.*, 1984; *Bruckler and Witono*, 1989; *Lin et al.*, 1994; *Ottlé and Vidal-Madjar*, 1994; *Saha*, 1995; *Houser et al.*, 1998], or as verification data [*Giacomelli et al.*, 1995]. The reasons for this are: (i) that remote sensing data is just beginning to gain acceptance in the hydrologic community as an operational tool for measuring the near-surface soil moisture content; (ii) assimilation of remote sensing data requires the development of land surface models that simulate soil moisture for a thin near-surface layer which is compatible with the nature of the remote sensing observations [*Lakshmi and Susskind*, 1997], and (iii) routine remote sensing of soil moisture content is not yet available. In addition, techniques for updating the land surface model with remote sensing data require investigation, and the near-surface soil moisture observations must be proven useful when used with land surface models [*Georgakakos and Baumer*, 1996].

This paper illustrates, using a numerical experiment with synthetic observation data, how remote sensing data might be used to initialize the soil moisture states in a global climate model. Moreover, it is shown how the soil moisture content, evapotranspiration and runoff forecasts

from a land surface model are improved when near-surface soil moisture data is assimilated into the land surface model. Furthermore, we observe that the structure of the land surface model modifies the effectiveness of the assimilation method.

2 MODELS

Previous studies have illustrated that an assimilation scheme having the characteristics of the Kalman filter is most effective for updating of the forecast land surface states [eg. *Houser et al.*, 1998; *Walker et al.*, 2001]. Such schemes have the advantage of being able to update more than just the observed state value, through the correlation with other states and state values in other locations. In this study, the Kalman filter assimilation scheme is used to update the soil moisture prognostic variables in the land surface model of *Koster et al.* [2000] with synthetic "observations" of the near-surface soil moisture content.

2.1 The (Extended) Kalman Filter

The Kalman filter assimilation method is a linearized statistical scheme that provides a statistically optimal update of the system states based on the relative magnitudes of the model system state estimate and observation covariances. The principal advantage of this approach is that the Kalman filter provides a framework within which the entire system is modified, with covariances representing the reliability of the observations and model prediction.

The Kalman filter algorithm [*Kalman*, 1960] tracks the conditional mean of a statistically optimal estimate of a state vector **X**, through a series of forecasting and update steps. To apply the Kalman filter, the equations for evolving the system states must be written in the linear state space formulation of (1). When these equations are non-linear, the Kalman filter is called the

extended Kalman filter, and is a first-order linearization approximation of the non-linear system. The forecasting equations are [*Bras and Rodriguez-Iturbe*, 1985]

$$\hat{\mathbf{X}}^{n+1/n} = \mathbf{A}^n \cdot \hat{\mathbf{X}}^{n/n} + \mathbf{U}^n + \left(\mathbf{w}^n\right) \quad (1)$$

$$\boldsymbol{\Sigma}_{\mathrm{x}}^{n+1/n} = \mathbf{A}^n \cdot \boldsymbol{\Sigma}_{\mathrm{x}}^{n/n} \cdot \mathbf{A}^{n^{\mathrm{T}}} + \mathbf{Q}^n \quad (2),$$

where **A** is the state propagation matrix relating the system states at times n+1 and n, **U** is a vector of forcing, **w** is the model error, $\boldsymbol{\Sigma}_{\mathrm{x}}$ is the covariance matrix of the system states and **Q** is the covariance matrix of the system noise (model error), defined as $\mathrm{E}[\mathbf{w}\cdot\mathbf{w}^{\mathrm{T}}]$. The notation n+1/n refers to the system state estimate at time n+1 from a forecasting step, and n/n refers to the system state estimate from either a forecasting or updating step at time n.

The covariance evolution equation consists of two parts: (i) propagation by model dynamics, and (ii) forcing by model error. The first, which is computationally the most demanding step in the Kalman filter algorithm, expresses how the dynamical processes in the forecast model affect the error covariance matrix. The second part of the covariance evolution equation represents the cumulative statistical effect of all processes that are external to, or not accounted for in the forecast model [*Dee*, 1991, 1995].

For the update step, the observation vector **Z** must be linearly related to the system state vector **X** through the transformation matrix **H**.

$$\mathbf{Z} = \mathbf{H} \cdot \hat{\mathbf{X}} + \mathbf{Y} + \left(\mathbf{v}\right) \quad (3),$$

where $\mathbf{Y}$ is the vector of state independent terms and $\mathbf{v}$ accounts for observation and linearization errors.

The best estimate of the system state vector $\hat{\mathbf{X}}$ is updated through the observation vector $\mathbf{Z}$ by means of Bayesian statistics. The system state vector and associated covariances are updated by the expressions [*Bras and Rodriguez-Iturbe*, 1985]

$$\hat{\mathbf{X}}^{n+1/n+1} = \hat{\mathbf{X}}^{n+1/n} + \mathbf{K}^{n+1}\left(\mathbf{Z}^{n+1} - \left(\mathbf{H}^{n+1}\cdot\hat{\mathbf{X}}^{n+1/n} + \mathbf{Y}^{n+1}\right)\right) \tag{4}$$

$$\mathbf{\Sigma}_{\mathrm{x}}^{n+1/n+1} = \left(\mathbf{I} - \mathbf{K}^{n+1}\cdot\mathbf{H}^{n+1}\right)\cdot\mathbf{\Sigma}_{\mathrm{x}}^{n+1/n}\cdot\left(\mathbf{I} - \mathbf{K}^{n+1}\cdot\mathbf{H}^{n+1}\right)^{\mathrm{T}} + \mathbf{K}^{n+1}\cdot\mathbf{R}^{n+1}\cdot\mathbf{K}^{n+1^{\mathrm{T}}} \tag{5},$$

where $\mathbf{I}$ is the identity matrix. The Kalman gain matrix $\mathbf{K}^{n+1}$ weights the observations against the model forecast. Its' weighting is determined by the relative magnitudes of model uncertainty embodied in $\mathbf{\Sigma}_{\mathrm{x}}^{n+1/n}$ with respect to the observation covariances $\mathbf{R}^{n+1}$, defined as $\mathrm{E}[\mathbf{v}\cdot\mathbf{v}^{\mathrm{T}}]$. The Kalman gain is given by

$$\mathbf{K}^{n+1} = \mathbf{\Sigma}_{\mathrm{x}}^{n+1/n}\cdot\mathbf{H}^{n+1^{\mathrm{T}}}\cdot\left(\mathbf{R}^{n+1} + \mathbf{H}^{n+1}\cdot\mathbf{\Sigma}_{\mathrm{x}}^{n+1/n}\cdot\mathbf{H}^{n+1^{\mathrm{T}}}\right)^{-1} \tag{6}.$$

The key assumptions in the Kalman filter are that: (i) the continuous time error process $\mathbf{w}$ is a Gaussian white noise stochastic process with mean vector equal to the zero vector and covariance matrix equal to $\mathbf{Q}$; and (ii) the discrete-time error sequence $\mathbf{v}$ is a Gaussian independent sequence with mean equal to zero and covariance equal to $\mathbf{R}$. The initial state vector $\hat{\mathbf{X}}^{0/0}$ is also assumed Gaussian with mean vector $\hat{\mathbf{X}}^{0/0}$ and covariance matrix $\mathbf{\Sigma}_{\mathrm{x}}^{0/0}$.

The Kalman filter model error forecasting equation in (2) is dependent upon: (i) an initial system state error covariance matrix $\mathbf{\Sigma}_x^{0/0}$; (ii) a model error forcing term **Q**; and (iii) the system state forecasting equation described by the linear state space formulation in (1). The system state error covariance matrix is often initialized using degree-of-belief estimates of the errors in initial states to specify the diagonal elements (variances) of the initial covariance matrix, with the off-diagonal elements (covariances) set to zero [*Georgakakos and Smith*, 1990]. The model error forcing term **Q** results from inaccurate specification of the model structure as a result of: (i) linearization of the model physics (including sub-grid variability); (ii) estimation errors in the values of model parameters; and (iii) measurement errors in the model input (eg. errors in precipitation). This is the most difficult component of the Kalman filter to identify correctly [*Georgakakos and Smith*, 1990]. Hence, this term is generally chosen ad-hoc [*Ljung*, 1979]. The variance of the observations **R** can be identified reliably in most cases, since it depends on the characteristics of the measuring device [*Georgakakos and Smith*, 1990].

2.2 The Land Surface Model

The land surface model used in this study is the catchment-based land surface model of *Koster et al*. [2000], illustrated schematically in Figure 1. It is a non-traditional land surface modeling framework that includes an explicit treatment of sub-grid soil moisture variability and its effect on runoff and evaporation. A key innovation in this approach is the shape of the land surface element. *Koster et al.*, [2000] abandon the traditional approach of defining quasi-rectangular land surface elements with boundaries defined by the overlying atmospheric grid. Instead, they define the fundamental land surface element to be the hydrological catchment, with boundaries defined by the topography. The catchments used in this application are at level 5 in the Pfafstetter system [*Verdin and Verdin*, 1999] with an average catchment area of 4400 km^2.

This land surface model uses TOPMODEL [*Beven and Kirkby*, 1979] concepts to relate the water table distribution to the topography. The consideration of both the water table distribution and non-equilibrium conditions in the root zone leads to the definition of three bulk moisture prognostic state variables (catchment deficit, root zone excess and surface excess) and a special treatment of moisture transfer between them. The framework of this land surface model provides a method for calculating the saturated, stressed (wilting) and unstressed fractions of the catchment and their respective soil moisture content from the three prognostic variables. Alternatively, the catchment average soil moisture content may be evaluated.

The catchment deficit is defined as the average amount of water per unit area that must be added to the catchments' soil to bring the entire catchment to saturation, assuming equilibrium conditions in the unsaturated zone. If equilibrium conditions could be assumed in the unsaturated zone, the catchment deficit by itself would be sufficient to characterize the catchments complete moisture state. To account for such non-equilibrium behavior, root zone and surface zone excess storages are introduced. These "excess" storages are the amount by which the moisture in the root and surface zones deviate from the moisture content implied by the local equilibrium moisture profile. While the catchment deficit distribution is described by the distribution of topographic index, there is no distribution presumed for the excess in the root and surface zones. However, as a result of the catchment deficit distribution, the root zone and surface zone soil moisture contents are spatially variable according to topography.

The catchment-based land surface model soil moisture prognostic variable forecasting equations are given by

$$srfexc^{n+1} = srfexc^{n} - srflow + i - es \tag{7}$$

$$rzexc^{n+1} = rzexc^{n} + srflow - rzflow - ev \tag{8}$$

$$catdef^{n+1} = catdef^{n} - rzflow + baseflow + et \tag{9},$$

where *srfexc* (m) is the surface excess, *rzexc* (m) is the root zone excess, *catdef* (m) is the catchment deficit and the superscript *n* is the time tag. The redistribution between the surface excess and root zone excess, *srflow* (m), and between the root zone excess and catchment deficit, *rzflow* (m), are given by

$$srflow = srfexc \cdot \frac{\Delta t}{\tau_1} \tag{10}$$

$$rzflow = rzexc \cdot \frac{\Delta t}{\tau_2} \tag{11},$$

where Δt (s) is the time step size, and $\tau_1 = f(srfexc, rzexc)$ and $\tau_2 = f(rzexc, catdef)$ are empirical moisture transfer timescale functions (s). The baseflow (m) is given by $baseflow = f(catdef)$, while the soil infiltration *i* (m), bare soil evaporation *es* (m), transpiration *ev* (m), and evapotranspiration *et* (m) are all described by functions of the form *f*(*srfexc*,*rzexc*,*catdef*). A complete description of this model is given in *Koster et al.* [2000] and *Ducharne et al.* [2000].

2.3 Application of the Kalman Filter

In this study, we have used a one-dimensional Kalman filter for updating the soil moisture prognostic variables of the catchment-based land surface model. A one-dimensional Kalman filter was used because of its computational efficiency and the fact that at the scale of catchments used, correlation between the soil moisture prognostic variables of adjacent catchments is only

through the large-scale correlation of atmospheric forcing. Moreover, all calculations for soil moisture in the land surface model are performed independent of the soil moisture in adjacent catchments.

2.3.1 Covariance Forecasting

Forecasting of the soil moisture covariance matrix using Kalman filter theory requires a linear forecast model. However, forecasting of the soil moisture prognostic variables (surface excess, root zone excess and catchment deficit) in the catchment-based land surface model is non-linear. Hence, forecasting of the soil moisture prognostic variables covariance matrix was achieved through linearization of the soil moisture forecasting equations. The linearization was performed by a first order Taylor series expansion of the non-linear forecasting equations (7-9). Using this approach, the covariance forecasting matrix is given by

$$\mathbf{A} = \begin{bmatrix} \frac{\partial srfexc^{n+1}}{\partial srfexc^{n}} & \frac{\partial srfexc^{n+1}}{\partial rzexc^{n}} & \frac{\partial srfexc^{n+1}}{\partial catdef^{n}} \\ \frac{\partial rzexc^{n+1}}{\partial srfexc^{n}} & \frac{\partial rzexc^{n+1}}{\partial rzexc^{n}} & \frac{\partial rzexc^{n+1}}{\partial catdef^{n}} \\ \frac{\partial catdef^{n+1}}{\partial srfexc^{n}} & \frac{\partial catdef^{n+1}}{\partial rzexc^{n}} & \frac{\partial catdef^{n+1}}{\partial catdef^{n}} \end{bmatrix} \quad (12).$$

Calculation of these derivatives may be done numerically, relieving the need for deriving analytical expressions. However, this results in an increased computational cost of approximately *m* times the analytical solution, where *m* is the number of dependent prognostic variables to be included in the assimilation.

For the initial covariance matrix, diagonal terms were specified to have a standard deviation of the maximum difference between the initial prognostic state value and the upper and

lower limits. This represents a large uncertainty in the initial soil moisture prognostic state values. In fact, the true initial soil moisture prognostic variable could be anywhere within the possible range. Off diagonal terms were specified to be zero initially, suggesting a zero correlation between the initial error in the three soil moisture prognostic state variables. The diagonal terms of the forecast model error covariance matrix **Q** were taken to be the predefined value given in Table 1, with the off diagonal terms taken to be zero. The assumption that errors in the three soil moisture prognostics resulting from errors in the model physics are independent is valid as the physics used for forecasting these three prognostic state variables are independent. This is unlike typical land surface models that vertically discretize the soil and apply the same physics to the soil moisture prognostic variables for each of the soil layers.

2.3.2 Kalman Filter Observation Equation

In order to perform an update of the soil moisture prognostic variables with the Kalman filter, the observation of near-surface soil moisture content must be linearly related to the soil moisture prognostic variables. In the land surface model used in this study, the soil moisture prognostic variables are the surface excess, root zone excess, and catchment deficit, and are related to the observed soil moisture of the surface layer θ_{srf} (v/v) through a complicated non-linear function:

$$\theta_{srf} = f_w(rzexc, catdef) + \frac{srfexc}{z_1} \quad (13),$$

where z_1 is the surface layer thickness (0.02 m). The complete expansion of this function is given in the Appendix. A first order Taylor series expansion of the non-linear function f_w allows for evaluation of the surface soil moisture equation

$$\{\theta_{srf}\} = \left\langle \frac{1}{z_1} \quad \frac{\partial f_w}{\partial rzexc} \quad \frac{\partial f_w}{\partial catdef} \right\rangle \begin{bmatrix} srfexc \\ rzexc \\ catdef \end{bmatrix} + \left\{ f_w^* - \frac{\partial f_w}{\partial rzexc} \cdot rzexc^* - \frac{\partial f_w}{\partial catdef} \cdot catdef^* \right\} \quad (14),$$

where the * refers to prognostic variable values about which the Taylor series expansion is evaluated.

3 NUMERICAL EXPERIMENTS

A set of numerical identical twin experiments have been undertaken for the entire continent of North America, in order to illustrate the effectiveness of the assimilation scheme in providing an accurate estimate of the soil moisture storage throughout the entire soil profile given periodic near-surface soil moisture observations. Such an estimate may then be used for the initialization of a global climate model. The corresponding influence of errors in soil moisture content on the forecast of evapotranspiration and runoff has also been illustrated. Finally, we observe that the structure of the land surface model and its linearization for covariance forecasting modifies the effectiveness of the assimilation.

3.1 Model Input Data

In this study, atmospheric forcing data and soil and vegetation properties from the first International Satellite Land Surface Climatology Project (ISLSCP) initiative [*Sellers et al*., 1996] have been used as model input for the year 1987. Such data includes: air temperature and humidity at two meters, surface wind speed, atmospheric pressure, precipitation, downward solar and longwave radiation, greenness, leaf area index, surface roughness length, surface snow free albedo, zero plane displacement height, vegetation class, soil porosity, soil depth and soil texture.

Soil properties not defined by ISLSCP were taken to be uniform across North America with the values given in Table 2. Catchment boundaries and topographic parameters were derived from a 30-arc-second (≈1 km) digital elevation model of North America from the United States Geological Survey EROS Data Center [*Ducharne et al.*, 2000]. The initial model states for 1987 in each of the 5018 catchments used to model the entire North America were determined by driving the model to equilibrium at the beginning of 1987 to avoid a non-equilibrated spin-up signal.

3.2 Observation and Evaluation Data

Using the land surface model of *Koster et al.* [2000], the initial conditions from spin-up, and the model input data described above, the temporal and spatial variation of soil moisture content across North America was forecast for 1987. The forecasts of near-surface soil moisture content were output once every 3 days to represent the near-surface soil moisture measurements from remote sensing satellites. In addition to soil moisture content (Figures 2 to 4), the land surface model provided estimates of total evaporation and runoff (Figure 11) for each of the catchments. This simulation provided the "true" soil moisture content and water balance data for comparison with degraded simulations both with and without assimilation. Moreover, it allowed evaluation of the effectiveness of assimilating near-surface soil moisture data for improving the land surface model forecasts of soil moisture content and water budget components, when initialized with poor initial conditions.

3.3 Results and Discussion

To illustrate the effect of soil moisture initialization errors on the model's prediction, and the effectiveness of the Kalman filter assimilation scheme, comparisons are made with a degraded simulation. In the degraded simulation, the initial conditions were taken from the spin-

up described above, with the exception that soil moisture prognostic variables were set to arbitrarily wet values uniformly across the entire North America. Using the degraded soil moisture initialization, the land surface model was run with the same atmospheric forcing data as used to derive the observation and evaluation data above. Two separate simulations were undertaken. The first used only the degraded initial conditions and forcing data, while the second assimilated the near-surface "observations" from the true simulation once every 3 days. The soil moisture forecasts from both of these simulations are compared with the true simulation in Figures 2 to 4, at the end of January, July and December, respectively. The limitation of using the same model to forecast the land surface states as is used to derive the observation and evaluation data (identical twin experiment) is the implied assumption that you have a perfect model and the observations are unbiased, which is rarely if ever the case in reality. By using a different model to derive the observation and evaluation data than that used to forecast the land surface states (fraternal twin experiment), this assumption may be offset. However, such a study was beyond the scope of this paper.

Figure 2a illustrates how poor the degraded soil moisture initial conditions were compared to the true simulation (Figure 2b), and that even after 1 month there was very little improvement of the degraded simulation towards the true simulation. Apart from the near-surface layer, there was very little change in the spatial distribution of soil moisture. This, however, may be contrasted with the soil moisture forecast using assimilation of near surface "observations" (Figure 2c). This simulation shows a very close agreement between the near-surface layers of the true simualtion and the assimilated forecast, as would be expected. Moreover, apart from a small portion of the North American interior, there is a good agreement between the soil moisture contents in both the root zone and entire soil profile.

By the end of July there was some improvement in the soil moisture forecast of the degraded simulation (Figure 3a) towards the true simulation (Figure 3b), but even after 12 months of simulation (Figure 4a) there was still a large portion of North America with significant errors in the soil moisture forecast. This improvement in the degraded simulation of soil moisture content was only observed for catchments located in the low latitudes, where evapotranspiration rates are high year round. The difference between the degraded and true soil moisture simulations is entirely due to the error introduced in the initial conditions. So the improvement in the degraded simulation is purely a result of land surface model spin-up. This is because soil moisture content is a bounded variable, with the effects of wrong initialization being lost whenever the soil dries out or becomes fully wet. In contrast to the degraded simulation, the soil moisture forecast with assimilation (Figure 3c) continued to track the true simulation for regions where the true soil moisture was already retrieved. Some small localized errors in the soil moisture forecast persisted at the end of July, but by the end of December (Figure 4c) very little error remained.

The location, magnitude, and persistence of errors in the soil moisture forecast can be seen more clearly in Figure 5. Errors in the soil moisture forecasts have persisted longer in some regions of North America than others, even though they are in the same climatic regime and had the same amount of initialization error. The correlation of each model parameter with the spatial distribution of error in soil moisture in the entire soil profile at the end of January was analyzed. It was found that the distribution of soil depth had the greatest correlation with this residual soil moisture error.

Figure 6 shows a plot of soil depth for North America. When comparing with Figure 5a (bottom row), particularly for soil depth greater than 3m, there is a distinct relationship between soil depth and error in soil moisture retrieval, especially for drier regions where the initial error was greater. Thus, the fact that deeper soil moisture is less physically connected with the surface soil moisture, leads to a reduced impact of surface soil moisture assimilation on the forecast of total soil moisture content. Although the correlation between a near-surface soil moisture measurement and that of the entire soil profile is small for regions with very deep soil, it is still greater than for traditional land surface models which use a vertical discretization of the soil profile [*Houser et al.*, 1998]. This is a result of the equilibrium profile assumption used in the catchment-based land surface model, where the catchment deficit prognostic variable is the basis for calculating the near-surface soil moisture content (see Appendix). Departures from this equilibrium profile are accounted for by the surface and root zone excess storages, which typically account for a much smaller contribution in the calculation of soil moisture content both near the soil surface and at depth.

The temporal evolution of error for the entire North American continent is given in Figures 7 and 8 for the degraded simulations without and with assimilation respectively. Figure 7 shows a slow but clear and consistent improvement in the soil moisture profile of the degraded simulation as a result of the land surface model spinning-up to the true initialization. However, even after twelve months there are still significant errors in soil moisture content for the entire soil profile. In contrast, Figure 8 shows a rapid initial improvement over the first month of assimilation, followed by a more gradual but none-the-less persistent improvement in soil moisture forecasts for both the root zone and entire soil profile. The assimilation scheme over-corrects the soil moisture forecast in the near-surface layer and root zone at the first update, but

this is rectified at the second update. After the second update, the assimilation scheme tracks the soil moisture content in the near-surface layer almost exactly. Moreover, the error in soil moisture forecasts for the three soil depths is negligible after around eight months of simulation.

A common approach to forecasting the model error covariance matrix using the Kalman filter is dynamics simplification [*Todling and Cohn*, 1994]. Using such an approach, only the dominant physical processes are used in forecasting of the error covariance matrix. In our application of the Kalman filter, the most obvious application of the dynamics simplification approach was to ignore the infiltration and evaporative terms from the prognostic equations (as these are the most difficult to linearize), focusing only on the redistribution of moisture within the soil. This assumes that the correlation between near-surface and deep soil moisture is strongly dependent on the redistribution between soil moisture storages and only weakly dependent to the external forcing. An alternative way to view this is to consider that infiltration and exfiltration is prescribed solely by the atmospheric conditions, and is independent of the soil moisture content.

The effect of using the dynamics simplification approach to forecasting the error covariance matrix in the catchment-based land surface model is demonstrated in Figure 9. The first 50 days of the time series is almost identical to that of Figure 8. However, beyond that both the root mean square error and mean error increase until about day 300. Moreover, the mean error time series shows a systematic error in the soil moisture forecasts of the near-surface layer, with the near-surface layer consistently drying too much and being topped up by the assimilation.

This deterioration in assimilated soil moisture is well correlated to the period of most active evapotranspiration in the Northern Hemisphere. The temporal variation of average evapotranspiration across North America is shown in Figure 10. Hence, the assumption that

correlation between near-surface soil moisture and the deeper soil moisture stores is only weakly dependent on the evapotranspiration is invalid.

The improvement in evapotranspiration and runoff prediction from the assimilation of near-surface soil moisture observations, over the simulation with degraded soil moisture content, is shown in Figure 11 for the month of July. Table 3 gives the mean daily evapotranspiration and runoff rates across North America for these simulations. The results show a large impact of incorrect soil moisture content on the prediction of evapotranspiration, which is the main feedback from the land surface model to the atmospheric model used in coupled runs of climate prediction. However, through the assimilation of near-surface soil moisture observations alone, we have illustrated that errors in evapotranspiration forecasts may be significantly reduced. Moreover, errors in the runoff component, which feeds back to the ocean model, may also be reduced.

4 CONCLUSIONS

A methodology for generating soil moisture initialization states for global climate models that does not rely on spinning-up the land surface model has been described. Rather, this methodology relies on the assimilation of remotely sensed observations of near-surface soil moisture content using a one-dimensional Kalman filter. A series of numerical experiments using the proposed methodology has illustrated that the true soil moisture content may be retrieved for the entire soil profile from remote sensing observations of the near-surface soil moisture content. Moreover, the effect of errors in soil moisture forecasts on the partitioning of atmospheric forcing into evapotranspiration and runoff has been illustrated.

This study found that the assimilation of near-surface soil moisture content works best for regions with shallower soils, particularly depths less than 3m. The soil moisture retrieval through assimilation still works for regions with greater soil depth, it just occurs more slowly. This is a direct result of the correlation between near-surface soil moisture content and soil moisture content at depth decreasing as the separation increases. Furthermore, we observe that the structure of the land surface model modifies the effectiveness of the assimilation method. The unique physics used in the catchment-based land surface model is well suited to the assimilation of near-surface soil moisture observations, as its dominant prognostic moisture state variable (catchment deficit) has a significant correlation with near-surface soil moisture content, except in very deep soils. Traditional land surface models generally have a vertical layering structure whose correlation is comparatively modest. This approach still works for other land surface models, but the improvement with depth occurs more slowly.

APPENDIX: Surface soil moisture calculations

The minimum soil wetness (volumetric soil moisture divided by porosity) $\omega_{rz_{min}}$ (–) in the root zone soil moisture distribution at equilibrium based on the catchment deficit *catdef* (m), with physical constraints $0 \le catdef \le \vartheta_{cd_{max}}$, is given by

$$\omega_{rz_{min}} = \gamma_4 + (1-\gamma_4)\frac{(1+\gamma_1 \cdot catdef_x)}{(1+\gamma_2 \cdot catdef_x + \gamma_3 \cdot catdef_x{}^2)} \quad (15),$$

where $\vartheta_{cd_{max}}$ (m) is the maximum catchment deficit, γ_i are topography related parameters defining the minimum root zone wetness to construct the root zone soil moisture wetness distribution [*Ducharne et al.*, 2000] and

$$catdef_x = \min(catdef, \vartheta_{cd_{lim}}) \quad (16).$$

The parameter $\vartheta_{cd_{lim}}$ (m) is a moisture threshold above which soil moisture is no longer controlled by TOPMODEL assumptions.

Integrating the root zone soil moisture distribution from $\omega_{rz_{min}}$ to infinity, the mean root zone soil wetness $\omega'_{rz_{eq}}$ (–) at equilibrium, based on $catdef_x$ being below $\vartheta_{cd_{lim}}$, is given by

$$\omega'_{rz_{eq}} = e^{-\alpha(1-\omega_{rz_{min}})} \cdot \left(\omega_{rz_{min}} - 1 - \frac{2}{\alpha}\right) + \omega_{rz_{min}} + \frac{2}{\alpha} \quad (17),$$

where α is a shape parameter used to construct the root zone soil wetness distribution as a function of $catdef_x$ and topography related parameters [*Ducharne, et al.*, 2000]. If the catchment

deficit is such that a water table no longer exists, the equilibrium mean root zone soil wetness $\omega'_{rz_{eq}}$ is ramped by a scaling factor such that

$$\omega_{rz_{eq}} = \omega_{wp} + \frac{\left(\omega'_{rz_{eq}} - \omega_{wp}\right)\cdot\left(\vartheta_{cd_{max}} - catdef\right)}{\vartheta_{cd_{max}} - \vartheta_{cd_{lim}}} \qquad catdef > \vartheta_{cd_{lim}} \qquad (18a)$$

$$\omega_{rz_{eq}} = \omega'_{rz_{eq}} \qquad catdef \le \vartheta_{cd_{lim}} \qquad (18b),$$

where ω_{wp} (–) is the wilting point soil wetness.

The mean non-equilibrium root zone soil wetness ω_{rz} (–) is calculated by adding the root zone excess storage *rzexc* (m), with physical constraints $\vartheta_{rz_{min}} - \vartheta_{rz_{eq}} \le rzexc \le \vartheta_{rz_{max}} - \vartheta_{rz_{eq}}$, such that

$$\omega_{rz} = \omega_{rz_{eq}} + \frac{rzexc}{\vartheta_{rz_{max}}} \qquad (19),$$

where $\vartheta_{rz_{min}}$ (m) and $\vartheta_{rz_{max}}$ (m) are the minimum and maximum soil moisture storage limits in the root zone respectively. Extrapolating the root zone soil wetness to the surface using an equilibrium profile assumption and then adding the surface excess storage *srfexc* (m), the surface soil moisture content θ_{srf}(v/v), with physical constraints $\theta_{wp} \le \theta_{srf} \le \phi$, may be calculated by

$$\theta_{srf} = \phi\cdot\left(\frac{\psi_{rz} - z_2}{\psi_{sat}}\right)^{\frac{-1}{b}} + \frac{srfexc}{z_1} \qquad (20),$$

where θ_{wp} (v/v) is the wilting point soil moisture, ϕ (v/v) is the soil porosity, b (–) is the *Clapp and Hornberger* [1978] soil texture parameter, z_1 (m) is the thickness of the surface layer, z_2 (m) is the distance from the midpoint of the surface layer to the midpoint of the root zone layer, ψ_{sat} (m) is the saturated soil matric potential and ψ_{rz} (m) is the root zone matric potential given by

$$\psi_{rz} = \psi_{sat} \cdot \omega_{rz}^{-b} \tag{21}.$$

ACKNOWLEDGEMENTS

This work was supported by funding from the NASA Seasonal-to-Interannual Prediction Project (NSIPP) NRA 98-OES-07. Support given by Randal Koster and Agnes Ducharne in application of the catchment-based land surface model is greatly appreciated.

REFERENCES

Beljaars, A.C.M., P. Viterbo, M.J. Miller, and A.K. Betts, The anomalous rainfall over the United States during July 1993: Sensitivity to land surface parameterization and soil anomalies, *Monthly Weather Review*, *124*, 362-383, 1996.

Beven, K.J. and M.J. Kirkby, A physically based, variable contributing area model of basin hydrology, *Hydrological Sciences - Bulletin*, *24*(1), 43-69, 1979.

Bras, R.L., and I. Rodriguez-Iturbe, *Random Functions and Hydrology*, Addison Wesley, Reading, Massachusetts, 559 pp, 1985.

Bruckler, L., and H. Witono, Use of remotely sensed soil moisture content as boundary conditions in soil-atmosphere water transport modeling: 2. Estimating soil water balance, *Water Resources Research*, *25*(12), 2437-2447, 1989.

Capehart, W.J., and T.N. Carlson, Decoupling of surface and near-surface soil water content: A remote sensing perspective, *Water Resources Research*, *33*(6), 1383-1395, 1997.

Clapp, R.B., and G.M. Hornberger, Empirical equations for some soil hydraulic properties, *Water Resources Research*, 14(4), 601-604, 1978.

Dee, D.P., Simplification of the Kalman filter for meteorological data assimilation, *Quarterly Journal of the Royal Meteorological Society*, *117*, 365-384, 1991.

Dee, D.P., On-line estimation of error covariance parameters for atmospheric data assimilation, *Monthly Weather Review*, *123*, 1128-1145, 1995.

Delworth, T.L., and S. Manabe, The influence of potential evaporation on the variabilities of simulated soil wetness and climate. *Journal of Climate*, *1,* 523-547, 1988.

Delworth, T., and S. Manabe, The influence of soil wetness on near-surface atmospheric variability, *Journal of Climate*, *2*, 1447-1462, 1989.

Ducharne, A., R.D. Koster, M.J. Suarez, M. Stieglitz, and P. Kumar, A catchment-based approach to modeling land surface processes in a GCM. Part 2: Parameter estimation and model demonstration, *Journal of Geophysical Research*, *105*(D20), 24823-24838, 2000.

Fast, J.D., and M.D. McCorcle, The effect of heterogenous soil moisture on a summer baroclinic circulation in the central United States, *Monthly Weather Review*, *119*, 2140-2167, 1991.

Georgakakos, K.P., and O.W. Baumer, Measurement and utilization of on-site soil moisture data, *Journal of Hydrology*, *184*, 131-152, 1996.

Georgakakos, K.P., and G.F. Smith, On improved hydrologic forecasting - Results from a WMO real-time forecasting experiment, *Journal of Hydrology*, *114*, 17-45, 1990.

Giacomelli, A., U. Bacchiega, P.A Troch, and M. Mancini, Evaluation of surface soil moisture distribution by means of SAR remote sensing techniques and conceptual hydrological modelling, *Journal of Hydrology*, *166*, 445-459, 1995.

Houser, P.R., W.J. Shuttleworth, J.S. Famiglietti, H.V. Gupta, K.H. Syed, and D.C. Goodrich, Integration of soil moisture remote sensing and hydrologic modeling using data assimilation, *Water Resources Research*, *34*(12), 3405-3420, 1998.

Jackson, R.D., S.B. Idso, and R.J. Reginato, Calculation of evaporation rates during the transition from energy-limiting to soil-limiting phases using albedo data, *Water Resources Research*, *12*(1), 23-26, 1976.

Jackson, T.J., T.J. Schmugge, A.D. Nicks, G.A. Coleman, and E.T. Engman, Soil moisture updating and microwave remote sensing for hydrological simulation, *Hydrological Sciences - Bulletin*, *26*(3), 305-319, 1981.

Kalman, R.E., A new approach to linear filtering and prediction problems. *Trans. ASME, Ser. D, J. Basic Eng., 82*, 35-45, 1960.

Koster, R.D., and M.J. Suarez, Relative contributions of land and ocean processes to precipitation variability, *Journal of Geophysical Research*, *100*(D7), 13775-13790, 1995.

Koster, R.D., M.J. Suarez, A. Ducharne, M. Stieglitz, and P. Kumar, A catchment-based approach to modeling land surface processes in a GCM. Part 1: Model structure, *Journal of Geophysical Research*, *105*(D20), 24809-24822, 2000.

Lakshmi, V., and J. Susskind, *Land surface hydrological processes using satellite data*. In: T.I. Stein (Editor), International Geoscience and Remote Sensing Symposium, Singapore, pp. 1102-1104, 1997.

Lin, D.S., E.F. Wood, P.A. Troch, M. Mancini, and T.J. Jackson, Comparisons of remotely sensed and model-simulated soil moisture over a heterogeneous watershed, *Remote Sensing of Environment*, *48*, 159-171, 1994.

Ljung, L., Asymptotic behaviour of the extended Kalman filter as a parameter estimator for linear systems, *IEEE Transactions on Automatic Control*, *AC-24*(1), 36-50, 1979.

Ottlé, C., and D. Vidal-Madjar, Assimilation of soil moisture inferred from infrared remote sensing in a hydrological model over the HAPEX-MOBILHY region, *Journal of Hydrology*, *158*, 241-264, 1994.

Prevot, L., R. Bernard, O. Taconet, D. Vidal-Madjar, and J.L. Thony, Evaporation from a bare soil evaluated using a soil water transfer model and remotely sensed surface soil moisture data, *Water Resources Research*, *20*(2), 311-316, 1984.

Raju, S., A. Chanzy, J. Wigneron, J. Calvet, Y. Kerr, and L. Laguerre, Soil moisture and temperature profile effects on microwave emission at low frequencies, *Remote Sensing of Environment*, *54*, 85-97, 1995.

Saha, S.K., Assessment of regional soil moisture conditions by coupling satellite sensor data with a soil-plant system heat and moisture balance model, *International Journal of Remote Sensing*, *16*(5), 973-980, 1995.

Sellers, P., B.W. Meeson, J. Closs, J. Collatz, F. Corprew, D. Dazlich, F.G. Hall, Y. Kerr, R. Koster, S. Loss, K. Mitchell, J. McManus, D. Myers, K.J. Sun, and P. Try, The ISLSCP Initiative I global data sets: Surface boundary conditions and atmospheric forcings for

land-atmosphere studies. *Bulletin of the American Meteorological Society, 77*, 1987-2005, 1996.

Shukla, J., and Y. Mintz, Influence of land-surface evapotranspiration on the earth's climate, *Science*, *215*, 1498-1501, 1982.

Todling, R., and S.E. Cohn, Suboptimal schemes for atmospheric data assimilation based on the Kalman filter, *Monthly Weather Review*, *122*, 2530-2557, 1994.

Verdin, K.L., and J.P. Verdin, A topological system for delineation and codification of the Earth's river basins, *Journal of Hydrology*, *218*, 1-12, 1999.

Walker, J.P., G.R. Willgoose, and J.D. Kalma, One-dimensional soil moisture profile retrieval by assimilation of near-surface observations: A comparison of retrieval algorithms, *Advances in Water Resources, 24*(6), 631-650, 2001.

LIST OF FIGURES

Figure 6: Spatial variation in total soil depth (mm) across the North American continent.

Figure 7: Temporal variation of error in soil moisture simulation with degraded initial conditions for soil moisture.

Figure 8: Temporal variation of error in soil moisture simulation with degraded initial conditions for soil moisture and assimilation of synthetic near-surface soil moisture observations.

Figure 9: Temporal variation of error in soil moisture simulation with degraded initial conditions for soil moisture and assimilation of synthetic near-surface soil moisture observations with only partial covariance forecasting.

Figure 10: Temporal variation of average evapotranspiration for North America.

Figure 11: Comparison of monthly average evapotranspiration (mm/d) for July 1987 from: a) degraded initial conditions for soil moisture; b) spin-up initial conditions (true simulation); and c) degraded initial conditions for soil moisture with assimilation of synthetic near-surface soil moisture observations from the true simulation once every 3 days. Comparison of monthly average runoff (mm/d) for July 1987 from: d) degraded initial conditions for soil moisture; e) spin-up initial conditions (true simulation); and f) degraded initial conditions for soil moisture with assimilation of synthetic near-surface soil moisture observations from the true simulation once every 3 days.

Table 1: Values for standard deviations of the forecast model error covariance matrix **Q** (mm/min).

srfexc	0.0025
rzexc	0.025
catdef	0.25

Table 2: Uniform soil properties specified for North America.

Saturated surface hydraulic conductivity	2.2×10^{-3} m s^{-1}
Transmittivity decay factor	3.26 m^{-1}
Saturated soil matric potential, ψ_{sat}	−0.281 m
Soil texture parameter, b	4
Root zone depth	1 m
Wilting point wetness, ω_{wp}	$0.148/\phi$

Table 3: Mean daily evaporation and runoff rates from the three simulations of North America in July 1987 (mm/d)

	Evapotranspiration	Runoff
Degraded simulation	2.95	0.79
True simulation	1.95	0.65
Degraded simulation with assimilation	2.01	0.65

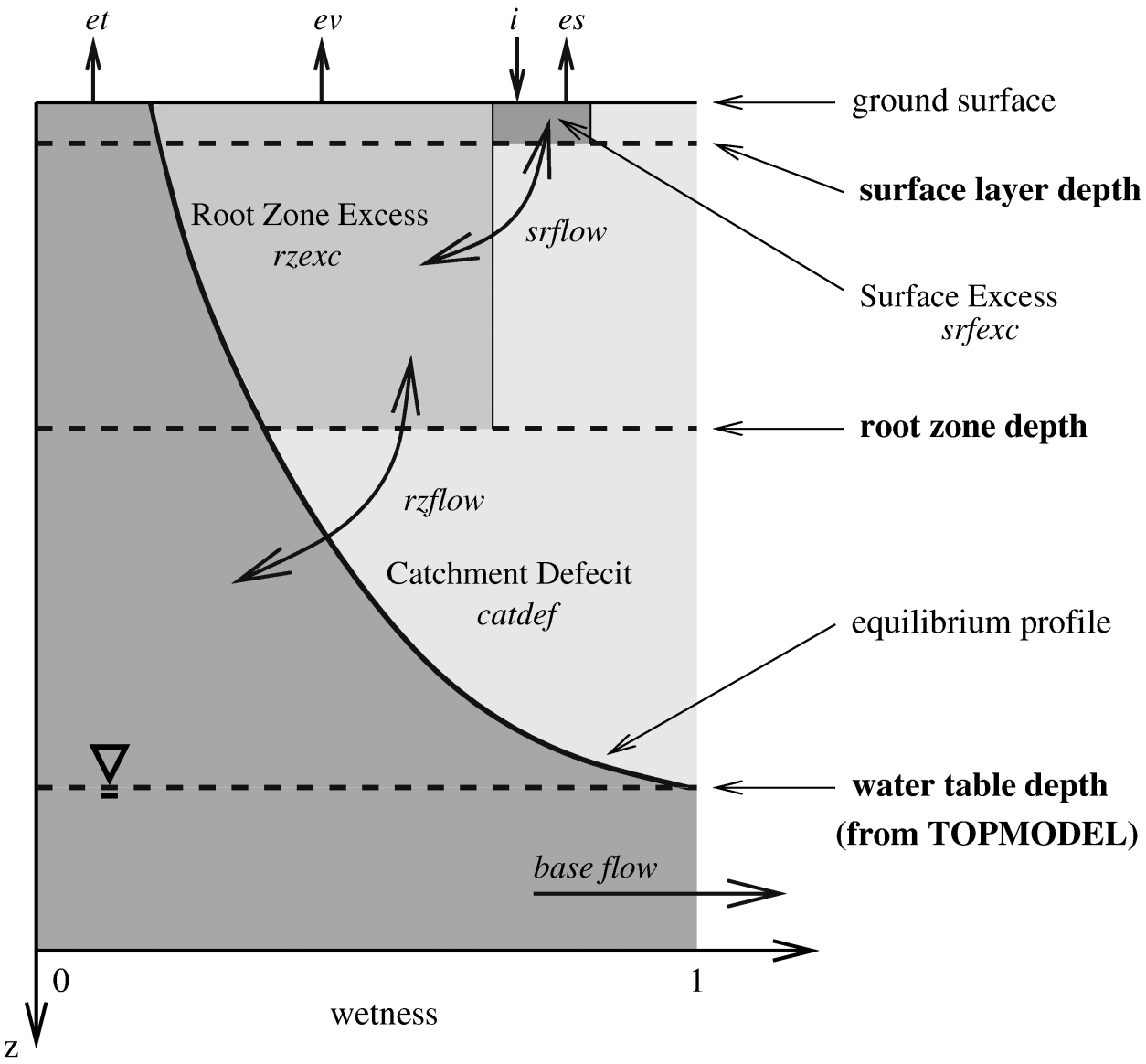
et
ev
i
es
ground surface
surface layer depth
Root Zone Excess
rzexc
srflow
Surface Excess
srfexc
root zone depth
rzflow
Catchment Defecit
catdef
equilibrium profile
water table depth
(from TOPMODEL)
base flow
0
1
wetness
z

Figure 1

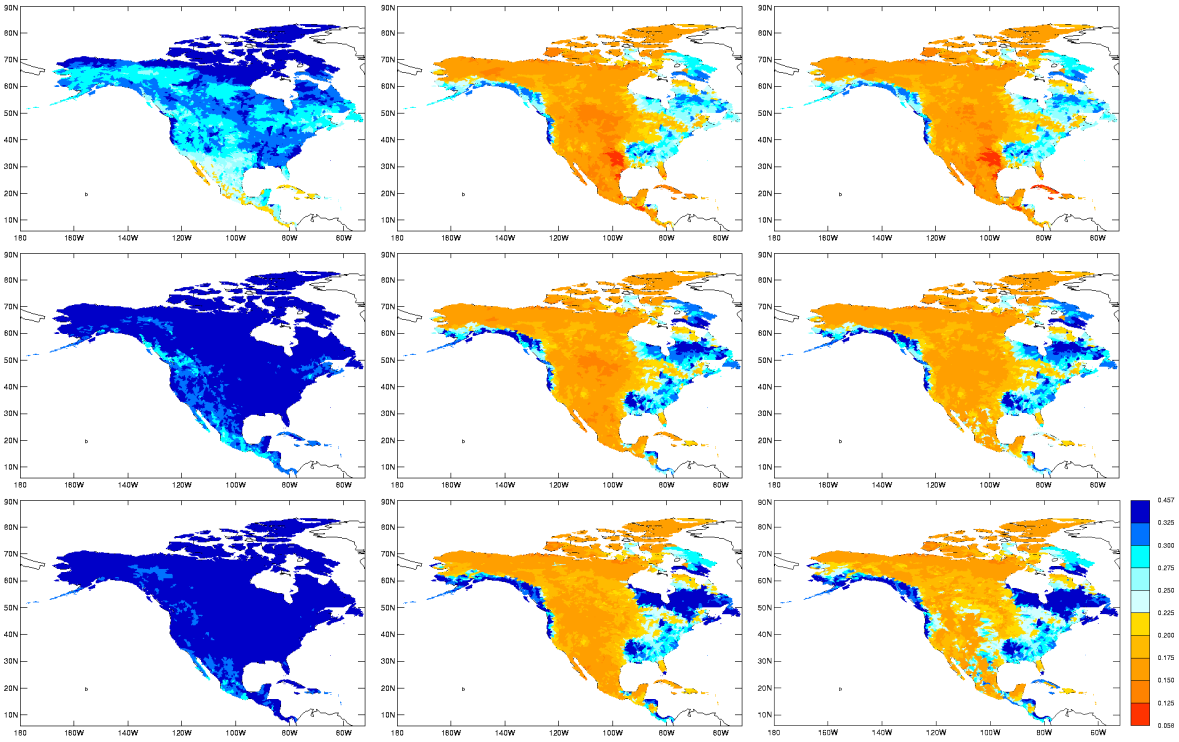

Figure 2

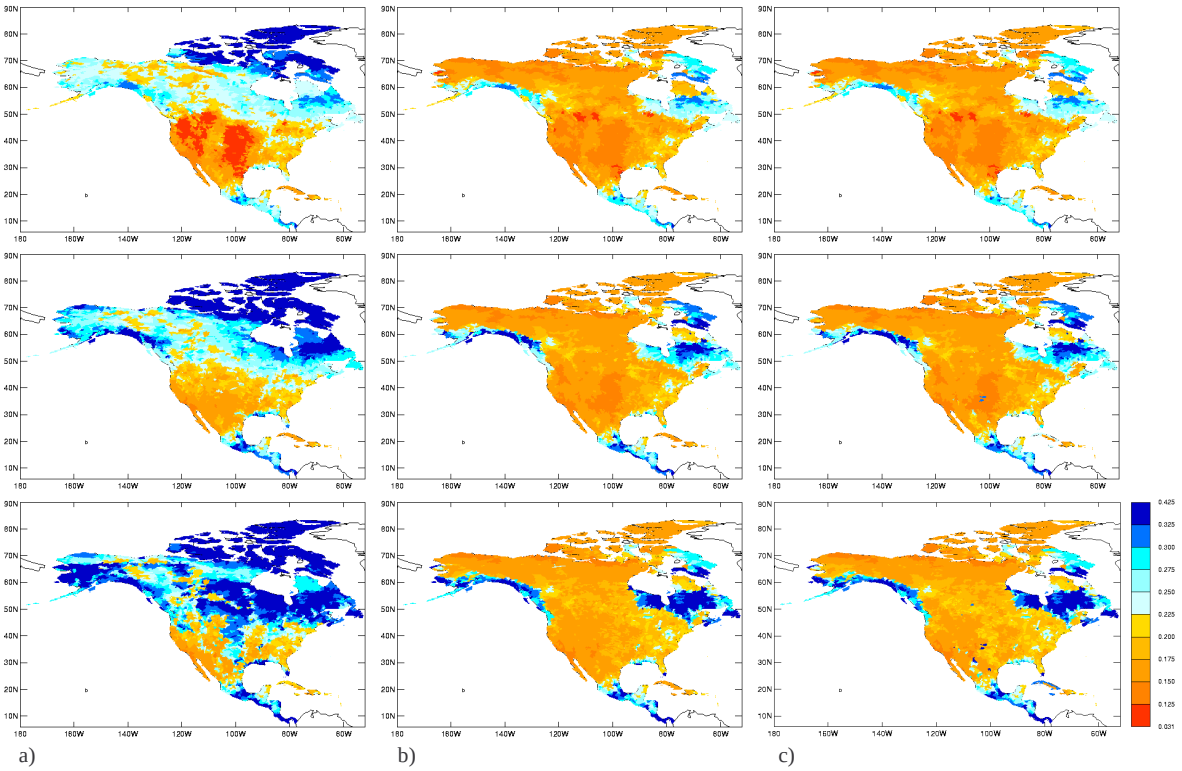

Figure 3

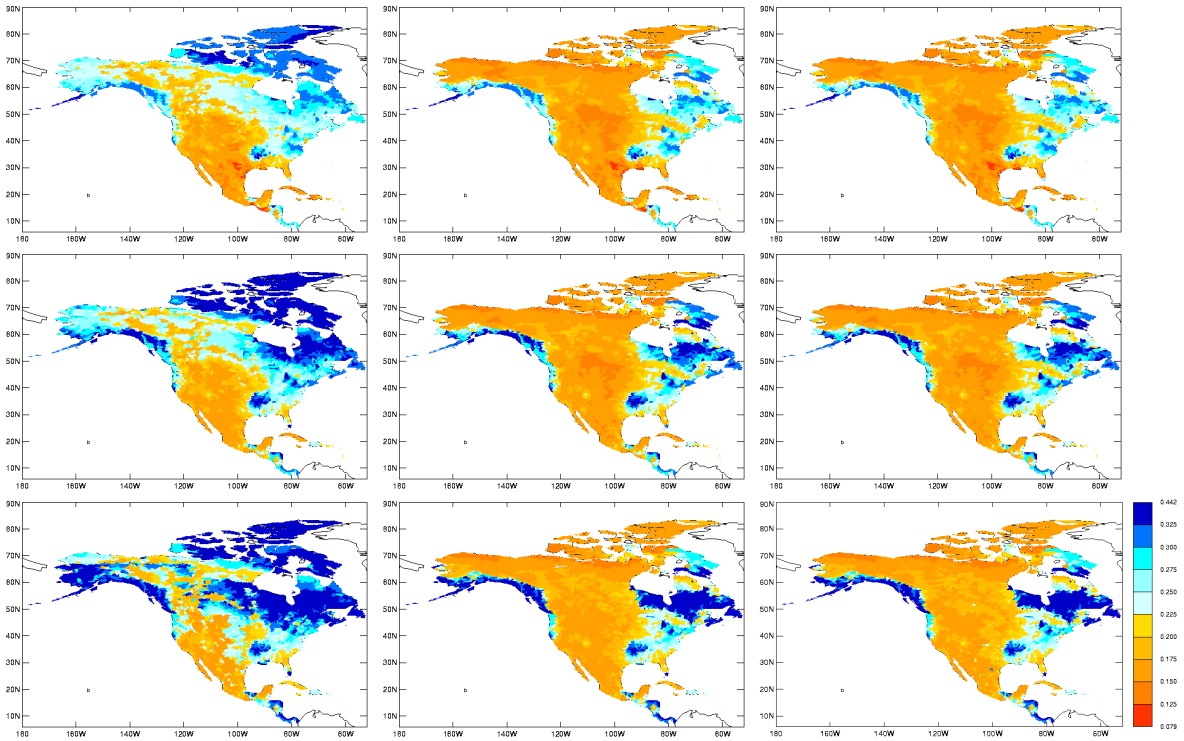

Figure 4

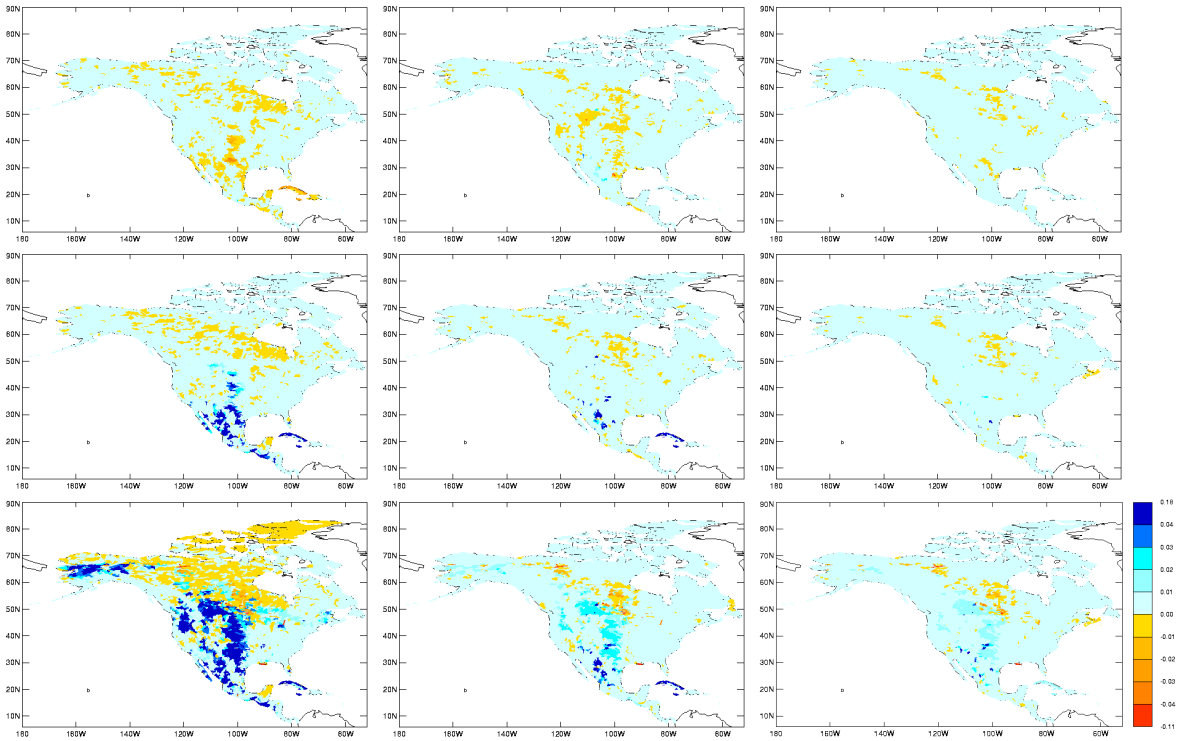

Figure 5

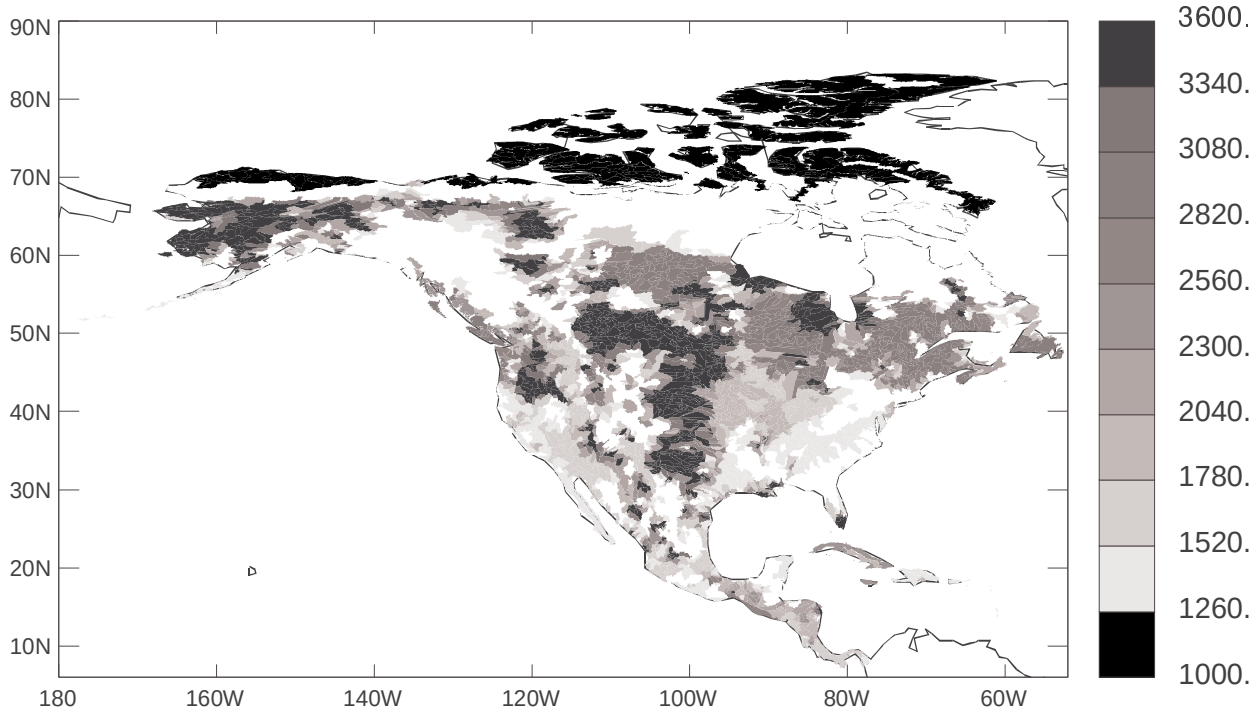
90N
80N
70N
60N
50N
40N
30N
20N
10N
180
160W
140W
120W
100W
80W
60W
3600.
3340.
3080.
2820.
2560.
2300.
2040.
1780.
1520.
1260.
1000.

Figure 6

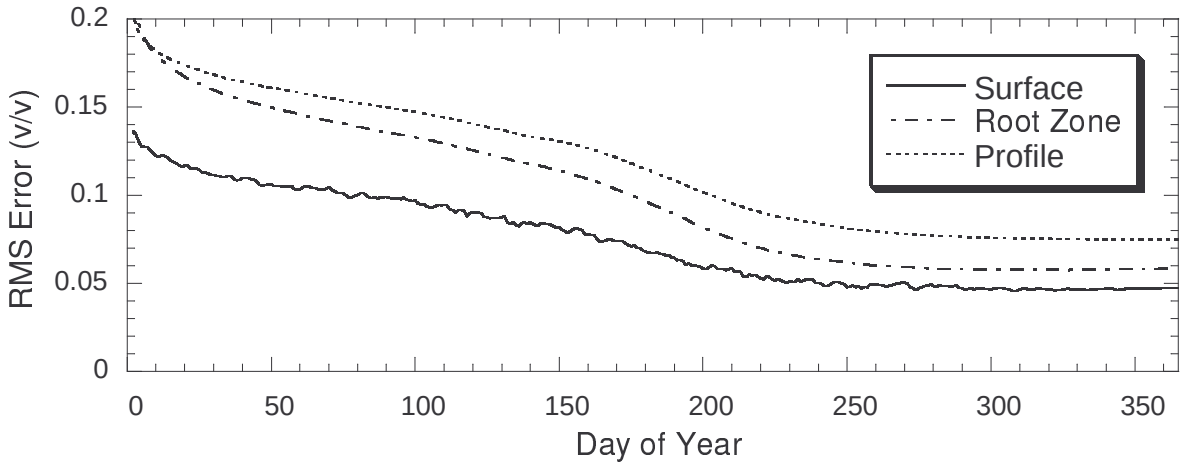
RMS Error (v/v)
0.2
0.15
0.1
0.05
0
0
50
100
150
200
250
300
350
Day of Year
Surface
Root Zone
Profile

a)

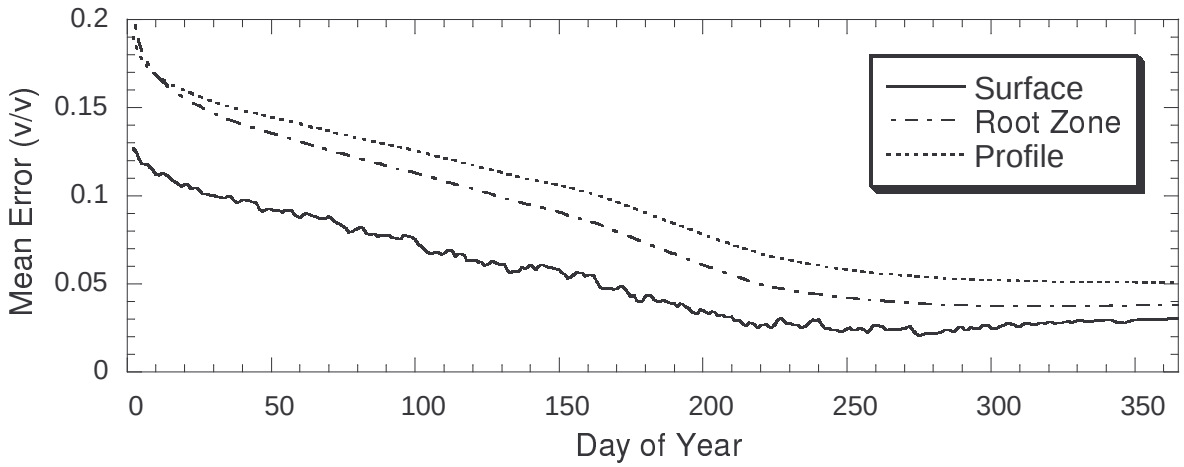
Mean Error (v/v)
0.2
0.15
0.1
0.05
0
0
50
100
150
200
250
300
350
Day of Year
Surface
Root Zone
Profile

b)

Figure 7

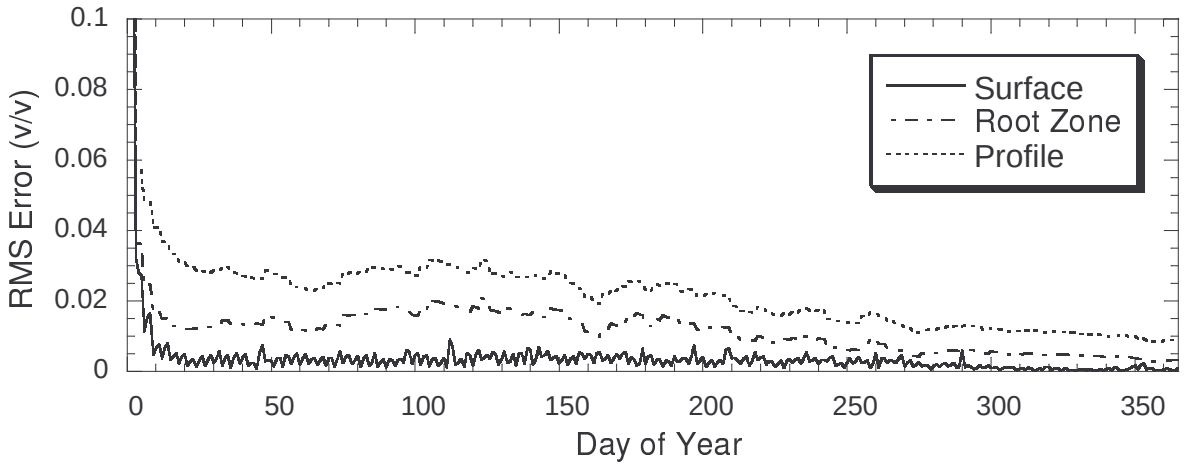
RMS Error (v/v)
0.1
0.08
0.06
0.04
0.02
0
0
50
100
150
200
250
300
350
Day of Year
Surface
Root Zone
Profile

a)

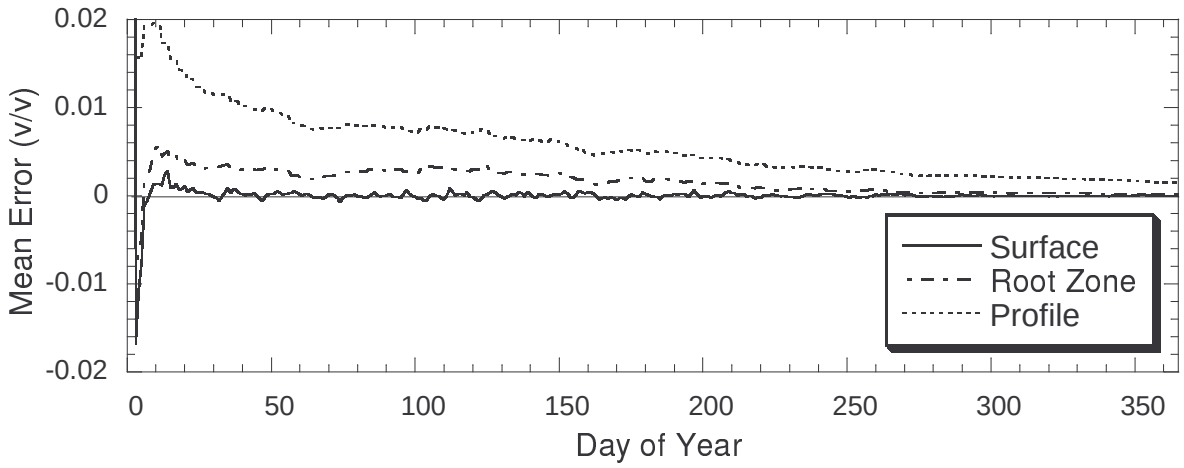
Mean Error (v/v)
0.02
0.01
0
-0.01
-0.02
0
50
100
150
200
250
300
350
Day of Year
Surface
Root Zone
Profile

b)

Figure 8

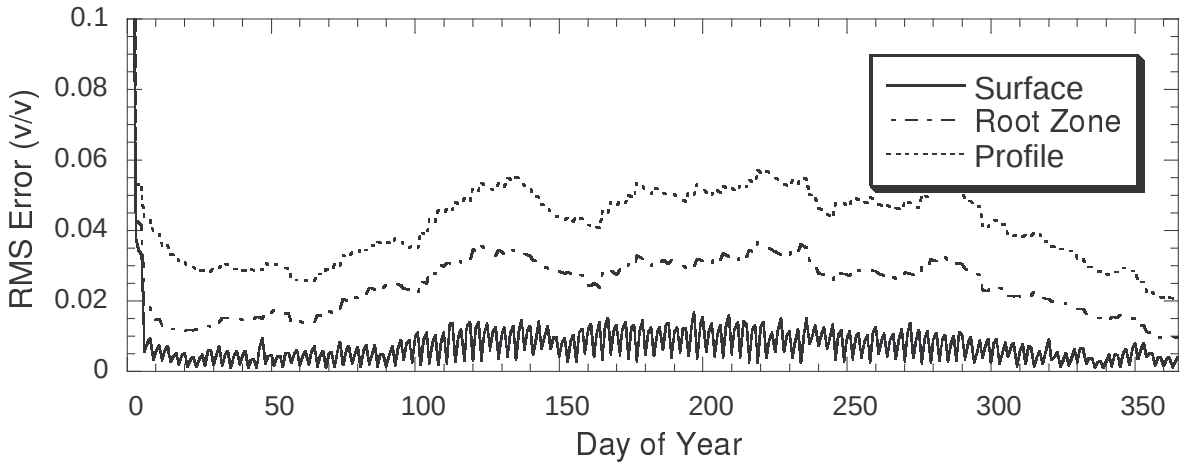
RMS Error (v/v)
0.1
0.08
0.06
0.04
0.02
0
0
50
100
150
200
250
300
350
Day of Year
Surface
Root Zone
Profile

a)

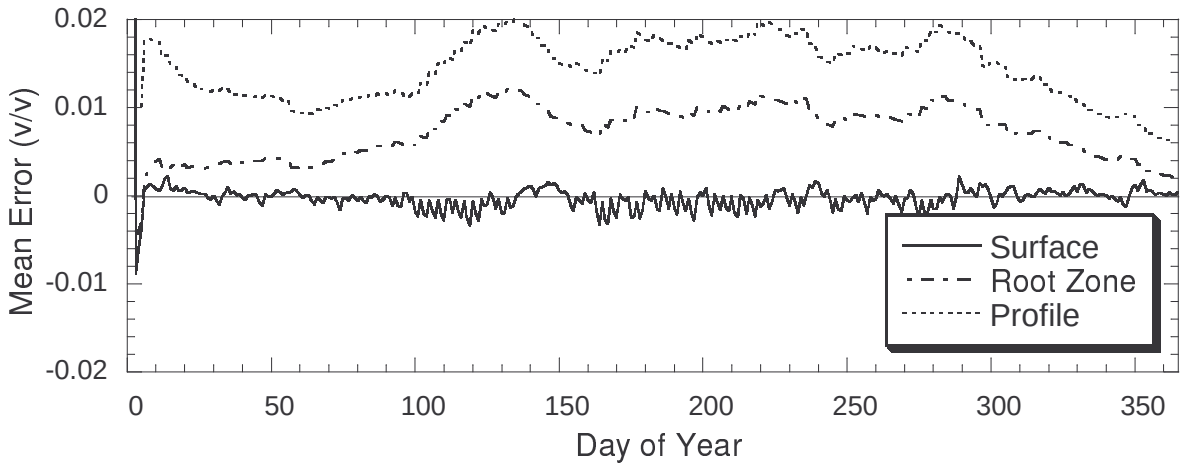
Mean Error (v/v)
0.02
0.01
0
-0.01
-0.02
0
50
100
150
200
250
300
350
Day of Year
Surface
Root Zone
Profile

b)

Figure 9

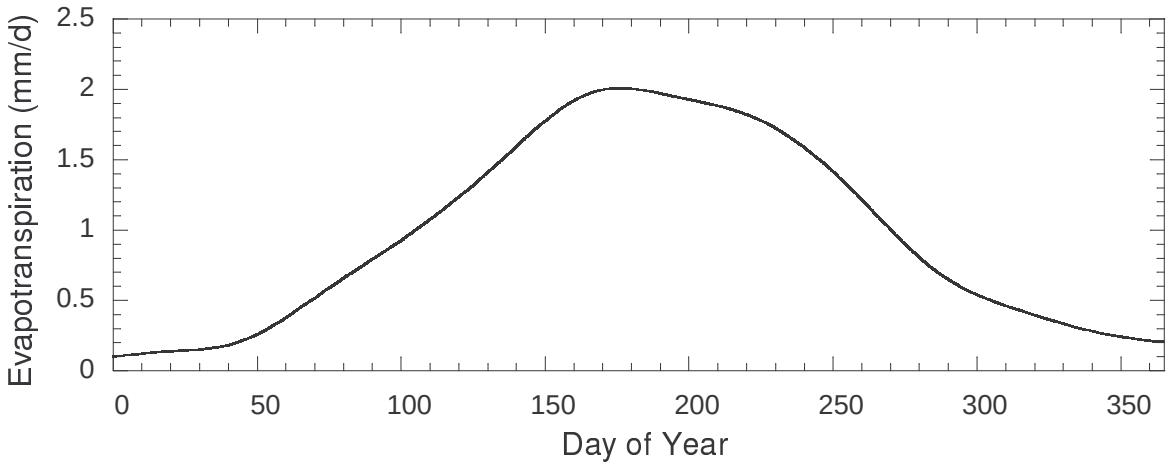
Evapotranspiration (mm/d)
2.5
2
1.5
1
0.5
0
0
50
100
150
200
250
300
350
Day of Year

Figure 10

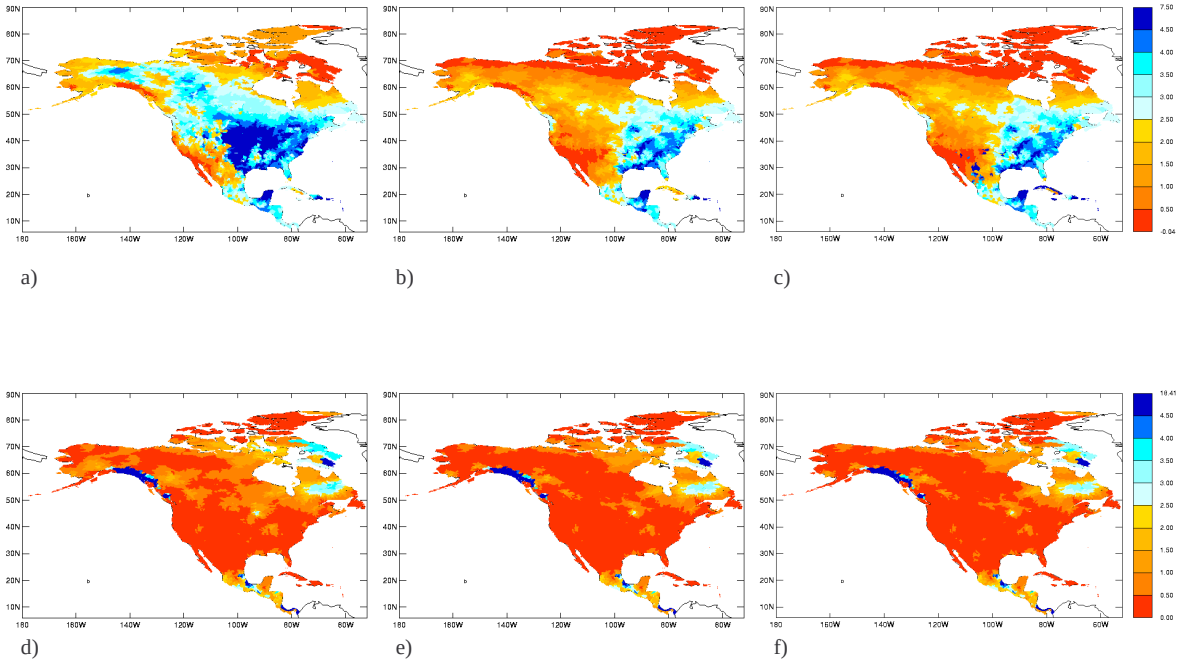

Figure 11